# The effect of diffusive nuclear burning in neutron star envelopes on cooling in accreting systems

Wijngaarden, M.J.P.; Ho, W.C.G.; Chang, P.; Page, D.; Wijnands, R.; Ootes, L.S.; Cumming, A.; Degenaar, N.; Beznogov, M.

**DOI**
10.1093/mnras/staa595

**Publication date**
2020

**Document Version**
Final published version

**Published in**
Monthly Notices of the Royal Astronomical Society

Monthly Notices
of the
ROYAL ASTRONOMICAL SOCIETY

MNRAS **493,** 4936–4944 (2020)
Advance Access publication 2020 March 18

doi:10.1093/mnras/staa595

# The effect of diffusive nuclear burning in neutron star envelopes on cooling in accreting systems

M. J. P. Wijngaarden [1★] Wynn C. G. Ho [1,2] Philip Chang,[3] Dany Page,[4] Rudy Wijnands,[5] Laura S. Ootes,[5] Andrew Cumming,[6] Nathalie Degenaar[5] and Mikhail Beznogov[4]

[1]*Mathematical Sciences and STAG Research Centre, University of Southampton, Southampton SO17 1BJ, UK*
[2]*Department of Physics and Astronomy, Haverford College, 370 Lancaster Avenue, Haverford, PA 19041, USA*
[3]*Department of Physics, University of Wisconsin-Milwaukee, 1900 E. Kenwood Blvd., Milwaukee, WI 53211, USA*
[4]*Instituto de Astronomía, Universidad Nacional Autónoma de México, Mexico City, 04510 Ciudad de México, CDMX, Mexico*
[5]*Anton Pannekoek Institute for Astronomy, University of Amsterdam, Postbus 94249, NL-1090 GE Amsterdam, the Netherlands*
[6]*Department of Physics, McGill Space Institute, McGill University, 3550 Rue University, Montreal, QC H3A 2T8, CanadaI confirm this.*

Accepted 2020 February 26. in original form 2020 January 22

## ABSTRACT

Valuable information about the neutron star (NS) interior can be obtained by comparing observations of thermal radiation from a cooling NS crust with theoretical models. Nuclear burning of lighter elements that diffuse to deeper layers of the envelope can alter the relation between surface and interior temperatures and can change the chemical composition over time. We calculate new temperature relations and consider two effects of diffusive nuclear burning (DNB) for H–C envelopes. First, we consider the effect of a changing envelope composition and find that hydrogen is consumed on short time-scales and our temperature evolution simulations correspond to those of a hydrogen-poor envelope within ∼100 d. The transition from a hydrogen-rich to a hydrogen-poor envelope is potentially observable in accreting NS systems as an additional initial decline in surface temperature at early times after the outburst. Second, we find that DNB can produce a non-negligible heat flux, such that the total luminosity can be dominated by DNB in the envelope rather than heat from the deep interior. However, without continual accretion, heating by DNB in H–C envelopes is only relevant for <1–80 d after the end of an accretion outburst, as the amount of light elements is rapidly depleted. Comparison to crust cooling data shows that DNB does not remove the need for an additional shallow heating source. We conclude that solving the time-dependent equations of the burning region in the envelope self-consistently in thermal evolution models instead of using static temperature relations would be valuable in future cooling studies.

**Key words:** dense matter – diffusion – stars: evolution – stars: neutron – X-rays: stars.

## 1 INTRODUCTION

Neutron stars (NSs) are an excellent laboratory for investigating extreme physics over a large range of densities, including supranuclear densities in their cores. One method to probe NS interiors is comparing theoretical models with observed temperatures of cooling NSs. If left undisturbed, isolated NSs cool over time after they are born hot in supernova explosions (see e.g. Potekhin, Pons & Page 2015). NSs in binary systems can occasionally undergo accretion outbursts, when new material is accreted from the companion star on to the NS surface. During an accretion outburst, the NS crust can be heated out of thermal equilibrium with the core as a sequence of non-equilibrium nuclear reactions in the crust, collectively known as *deep crustal heating*, are triggered when the underlying material is compressed by newly accreted matter (Haensel & Zdunik 1990; Brown, Bildsten & Rutledge 1998). After the accretion outburst, the NS crust cools back to thermal equilibrium with the core on time-scales of years (see, e.g, Wijnands, Degenaar & Page 2017 for a review). This means that the cooling phase can be covered with multiple observations during which the surface temperature can be measured to constrain theoretical cooling curves, which is a useful opportunity to gain insight in the properties and physics of the NS crust and core (e.g. Page & Reddy 2013; Cumming et al. 2017; Brown et al. 2018).

★ E-mail: m.j.p.wijngaarden@soton.ac.uk

For several crust cooling sources, the high observed surface temperatures $\lesssim$100 d after the accretion outburst cannot be explained using the standard deep crustal heating model but require the presence of an additional shallow heating source (at densities $\rho < 10^{11}$ g cm$^{-3}$) during outburst. Typically, during the outbursts, an amount of ∼1–2 MeV per accreted nucleon of shallow heating is needed to explain the observed cooling curves after the outbursts are over (e.g. Brown & Cumming 2009; Degenaar et al. 2014; Merritt et al. 2016), but for one source (MAXI J0556−332) as much as ∼17 MeV nucleon$^{-1}$ was needed (Homan et al. 2014; Deibel et al. 2015; Parikh et al. 2017). This means that the amount of shallow heating can be larger than that due to deep crustal heating, which releases ∼2 MeV nucleon$^{-1}$. One of the outstanding problems in cooling studies is the unknown physical mechanism of this shallow heat (see the discussion in Deibel et al. 2015). Thus, it is useful to explore additional heating mechanisms that are currently not accounted for in the present crustal heating models.

One of the challenges in understanding crust cooling and shallow heating is obtaining the interior temperature (at the bottom of the envelope) from observations of the surface emission. The relation between surface temperature and interior temperature is set by the heat conducting properties of the thin outer envelope ($\rho < \rho_b = 10^8$–$10^{10}$ g cm$^{-3}$), which is highly sensitive to chemical composition (Gudmundsson, Pethick & Epstein 1983; Potekhin, Chabrier & Yakovlev 1997; Brown, Bildsten & Chang 2002). NS cooling codes typically calculate the interior structure and thermal evolution from the centre of the star out to the bottom of the envelope (at $\rho_b$). Then, analytic fits of the temperature relations between the NS surface temperature ($T_s$) and the temperature at the bottom of the envelope, $T_b$ [$\equiv T(\rho_b)$], are used as a boundary condition. Analytic fits to numerical envelope calculations for different static envelope compositions and envelope sizes have been calculated for one (Gudmundsson et al. 1983) and two or more chemical component models (see e.g. Potekhin et al. 1997, 2003; Beznogov, Potekhin & Yakovlev 2016; Wijngaarden et al. 2019).

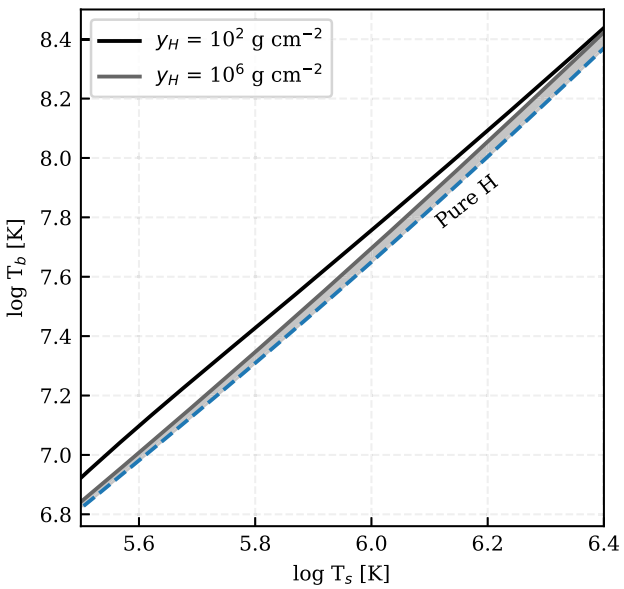


**Figure 1.** The $T_s$–$T_b$ relation for the H–C envelope with $\rho_b = 10^{10}$ g cm$^{-3}$. The solid line corresponds to both the model with and without DNB, as they are indistinguishable. The blue dashed line corresponds to a hydrogen column of $10^{10}$ g cm$^{-2}$ when DNB is not included. The grey shaded region corresponds to the grey region in Fig. 2 and shows the region in the $T_s$–$T_b$ relations that is excluded by taking DNB into account as the build-up of those hydrogen columns are prevented by nuclear burning.

Diffusive nuclear burning (DNB) of hydrogen and helium can affect the envelope $T_s$–$T_b$ relations and can alter the envelope composition over time. DNB occurs when lighter elements diffuse to depths where the temperature and density are large enough to ignite nuclear burning of these elements. This process has been studied for H–C (Chang & Bildsten 2003, 2004) and He–C envelopes (Chang, Bildsten & Arras 2010). In addition, Wijngaarden et al. (2019) calculated H–He and He–C temperature relations including the effect of DNB and investigated how DNB can alter the envelope composition over time for cooling isolated NSs.

Here we obtain analytic temperature relations for H–C envelopes and explore the effect of DNB on the observed cooling of NSs after an accretion outburst. The temperatures in the envelope after accretion outbursts are sufficiently large such that the heat deposited in the envelope by DNB may not be negligible, as was assumed in previous works. We investigate whether the common assumption in cooling studies that no energy is generated in the envelope during quiescence and that its composition does not change significantly during the cooling time is valid when DNB is taken into account. We compare the luminosity generated by DNB in the envelope when the NS is cooling to the interior luminosity, to explore the role of DNB as an additional heating mechanism. We consider how the envelope composition changes over time due to the consumption of lighter elements, which by itself can alter the observed cooling curves as the heat conduction properties of the envelope are sensitive to its chemical composition.

## 2 H–C ENVELOPES

### 2.1 $T_s$–$T_b$ relations

We calculate new temperature relations that include DNB for an H–C envelope with $\rho_b = 10^{10}$ g cm$^{-3}$. These temperature relations were calculated by computing a grid of envelope models for different combinations of surface temperatures and hydrogen columns and fitting an analytic relation to these results. More details on this approach can be found in Appendix A and in Wijngaarden et al. (2019). In Fig. 1, we show the resulting relation between surface temperature and bottom boundary temperature for varying hydrogen column sizes. For an H–C mixture, increasing the hydrogen column leads to a better heat-conducting envelope (i.e. the same bottom boundary temperature corresponds to a larger surface temperature). Note that increasing the hydrogen column in an H–He envelope has the opposite effect (see e.g. Beznogov et al. 2016). Analytic fits for the $T_s$–$T_b$ relations as a function of hydrogen column size ($y_H$) and scalable by surface gravity are given in Appendix A.

The $T_s$–$T_b$ relation is highly sensitive to the composition in the *sensitivity strip* of the envelope (where the dominant opacity changes between radiative and conductive). Thus when the change in hydrogen column size does not affect the composition in the sensitivity strip, the effect on the $T_s$–$T_b$ relation is negligible. This is shown in Fig. 2, where we explore the parameter space of $T_s$ and $y_H$ and show for which values the temperature relations are sensitive to $T_s$ and $y_H$. The red and blue regions in Fig. 2 show for which hydrogen column sizes the temperature relations are insensitive to further changes in column size and correspond to the maximum and minimum $T_b$ for a given $T_s$, respectively.

Including DNB leads to a clear upper limit on the hydrogen column size, as the build-up of larger columns is prevented by rapid hydrogen burning. Similar to what was found for H–He envelopes,

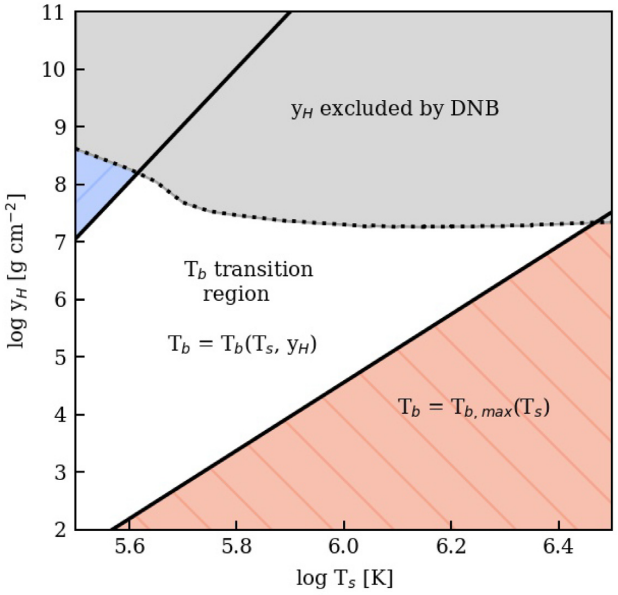


**Figure 2.** $T_s$–$y_H$ parameter space for the H–C envelope model with $\rho_b = 10^{10}$ g cm$^{-3}$. The solid lines enclose the region where the boundary temperature is sensitive to the hydrogen column density, i.e. $T_b = T_b(T_s, y_H)$. In this region, for a given $T_s$ and increasing $y_H$, the boundary temperature changes from that corresponding to a pure carbon envelope (red), where $T_b = T_{b,max}(T_s)$, to that of a pure hydrogen envelope (blue), where $T_b = T_{b,min}(T_s)$. Further changes in the hydrogen column outside of the transition region have negligible effect on the $T_b$–$T_s$ relations. The grey shaded region shows the parameter space that is excluded due to DNB (see text). Note that at large $y_H$, some excluded hydrogen columns overlap with the transition region. This means that the range in $T_b$ is smaller when DNB is taken into account.

we find that hydrogen columns $>10^7$ g cm$^{-2}$ cannot be sustained when DNB is taken into account. Note that for most temperatures, this means that a large portion of hydrogen columns located in the transition region are unphysical, leading to a smaller range in allowed boundary temperatures for a given surface temperature. The boundary temperatures corresponding to the excluded hydrogen columns (see Fig. 2) are highlighted in grey in Fig. 1. As shown by Figs 1 and 2, the main effect of DNB for the temperature relations is not the alteration of the composition profile in the sensitivity strip, but the introduction of naturally excluded hydrogen column sizes.

## 3 DNB LUMINOSITY

We compare the total DNB energy deposited in the envelope to the luminosity flowing from the interior (i.e. from any layer deeper than the envelope). The energy generated by DNB is converted to a total DNB luminosity by integrating the local energy generation rate over the mass in the envelope:

$$L_{\rm DNB} = \int \epsilon \, {\rm d}m = \int \epsilon 4\pi R^2 \, {\rm d}y \, {\rm erg \, s^{-1}}, \quad (1)$$

where $M$ is the total mass of the star, and the mass interval d$m$ is converted to column density interval d$y$ following Gudmundsson et al. (1983). The local energy generation rate is calculated as

$$\epsilon = \sum \frac{Q_i r_i}{\rho} \, {\rm erg \, g^{-1} \, s^{-1}}, \quad (2)$$

where $Q_i$ is the energy released by a reaction of type $i$, $r_i$ is the reaction rate of reaction type $i$, and $\rho$ is the local density. The luminosity flowing from the interior through envelope is typically assumed to be constant, such that the luminosity at the surface is $L_{\rm int} = L_s = 4\pi R^2 \sigma T_s^4$ that can be used as a boundary condition in thermal evolution codes (see e.g. Chamel & Haensel 2008; Brown & Cumming 2009; Page & Reddy 2013; Potekhin et al. 2015).

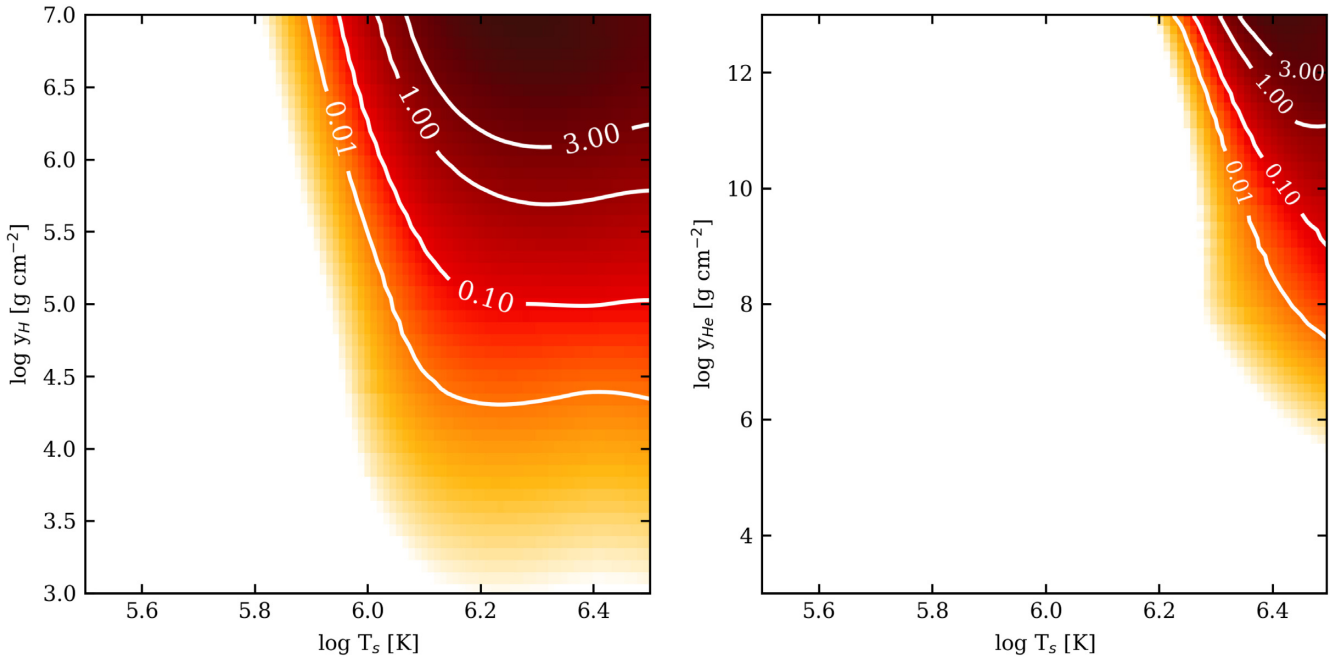


**Figure 3.** The explored $T_s$–$y_{\rm light}$ parameter space for H–C envelopes (left) and He–C envelopes (right). The colour is set by the ratio between the diffusive nuclear burning (DNB) luminosity and blackbody luminosity ($L_{\rm DNB}/L_{\rm int}$, where $L_{\rm int} = L_s = 4\pi R^2 \sigma T_s^4$). The coloured region shows where the luminosity due to DNB in the envelope becomes relevant compared to the blackbody luminosity for varying surface temperatures and light element columns. The contour line corresponding to unity indicates where $L_{\rm DNB}$ becomes larger than $L_{\rm int}$. The figure parameter ranges are chosen to match relevant values of surface temperatures and light element column densities in crust cooling studies.

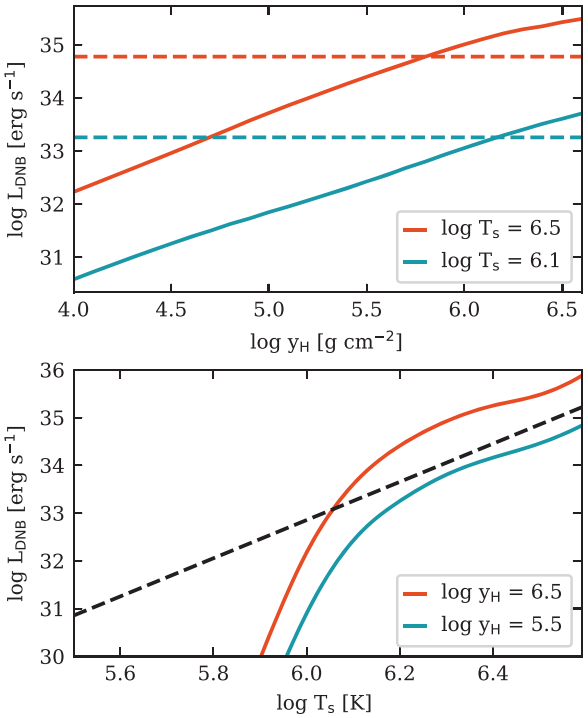


**Figure 4.** The DNB luminosities in an H–C envelope, for varying column densities (top) and temperatures (bottom). The luminosities corresponding to the surface temperatures are shown as dashed lines for comparison.

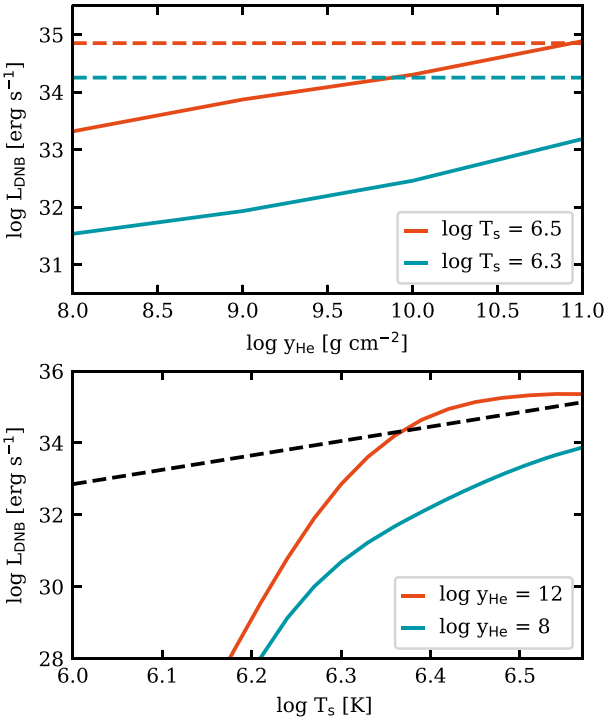


**Figure 5.** The DNB luminosities in an He–C envelope, for varying column densities (top) and temperatures (bottom). The luminosities corresponding to the surface temperatures are shown as dashed lines for comparison.

In Fig. 3, we show conditions ($T_s$, $y_{light}$) when the nuclear burning luminosity becomes relevant by computing the ratio $L_{DNB}/L_{int}$ for $y_{light} = y_H$ (left) and $y_{light} = y_{He}$ (right). For H–C envelopes, the dominant nuclear reactions are proton captures, which efficiently produce heat for a relatively large part of the $y_H$–$T_s$ parameter space. For surface temperatures above $\sim 10^6$ K and hydrogen columns larger than $\sim 10^5$ g $cm^{-2}$, the energy deposited by nuclear burning becomes comparable to and larger than the interior luminosity (see left-hand panel in Fig. 3). The hydrogen column densities and surface temperatures where the DNB luminosity becomes non-negligible are in the range inferred from observations of NSs in low-mass X-ray binaries (LMXBs) after accretion outbursts (see Wijnands et al. 2017 for an observational overview). In Fig. 4, we show the magnitude of the nuclear burning luminosity for varying hydrogen column (for $T_s = 1.26 \times 10^6$ and $3.16 \times 10^6$ K) in the top panel, and varying surface temperature in the bottom panel (for $y_H = 3.16 \times 10^4$ and $3.16 \times 10^6$ g $cm^{-2}$). As an initially large hydrogen column after an accretion episode is not unlikely, the energy deposited in the envelope by DNB could affect the surface temperature evolution after the outburst.

For He–C envelopes, where the dominant nuclear reactions are highly temperature sensitive $\alpha$-captures, the heat generated by nuclear reactions is only relevant for very high temperatures, $T_s > 2 \times 10^6$ K, and helium columns, $y_{He} \gtrsim 10^9$ g $cm^{-2}$, as is shown in the right-hand panel of Fig. 3. In this regime, the luminosity from nuclear burning becomes larger than $10^{34}$ erg $s^{-1}$, as is shown in Fig. 5. For smaller columns and temperatures, the nuclear burning luminosity rapidly drops and is negligible compared to the interior luminosity (indicated by the dashed lines). The nuclear burning luminosity is relevant compared to the interior luminosity (indicated by the dashed lines) for a smaller range of (and at significantly higher) surface temperatures and column densities compared to H–C envelopes.

## 4 DNB EFFECT ON POST-OUTBURST COOLING CURVES

We investigate the heating effect of DNB on the post-outburst temperature evolution of a cooling NS crust. We simulate the accretion outburst to obtain the post-outburst interior luminosity evolution using the relativistic cooling code NSCool (Page 2016) for a NS with mass $M = 1.4$ $M_\odot$ and radius $R = 11.5$ km. The outer boundary condition (at the bottom of the envelope, $\rho_b$) of the cooling code is that the interior luminosity at $\rho_b$ is the same as the luminosity at the surface (i.e. no energy is generated or lost in the envelope): $L_s = L_{int}$. Thus, we obtain the surface temperature without DNB ($T_{s,old}$) directly from $L_{int}$. In the following, we will assume the heat generated by DNB in the low-density envelope flows towards the surface and DNB does not affect the interior luminosity. Therefore, we can calculate the heating effect of DNB by post-processing the interior luminosity and surface temperature evolution from NSCool.

We convert the surface temperature without DNB ($T_{s,old}$) to a surface temperature with DNB ($T_s$) using $L_s = L_{int} + x_{out} L_{DNB}$, where $L_{DNB}$ is the DNB luminosity and we introduce $x_{out}$ as the fraction of DNB luminosity that is radiated outwards so that it is easy to investigate the effect of relaxing our assumption of $x_{out} = 1$. The resulting surface temperature including the heat generated by DNB can then be calculated as

$$T_s = T_{s,old} \left(1 + \frac{x_{out} L_{DNB}}{L_{int}}\right)^{1/4}. \quad (3)$$

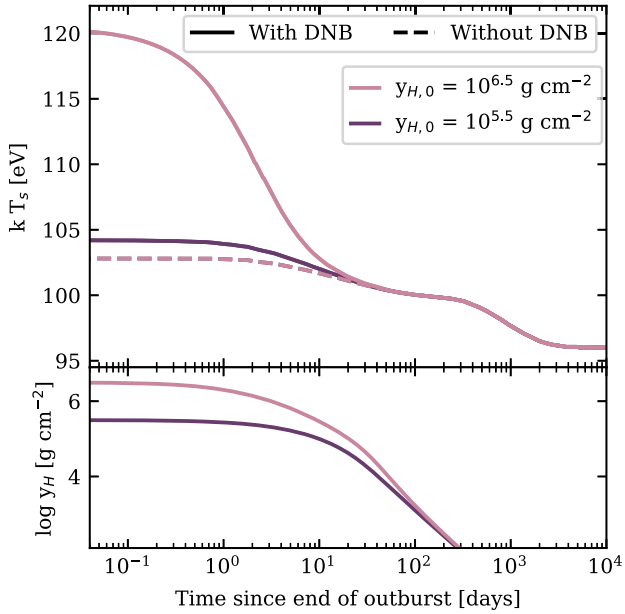


**Figure 6.** Comparison of the post-outburst surface temperature evolution with (solid) and without (dashed) additional DNB heating for different initial hydrogen columns (see line colours). The interior luminosity was calculated using an outburst duration of 1 yr and $\dot{M} = 10^{17}\,\mathrm{g\,s^{-1}} \approx 2 \times 10^{-9}\,\mathrm{M_\odot\,yr^{-1}}$.

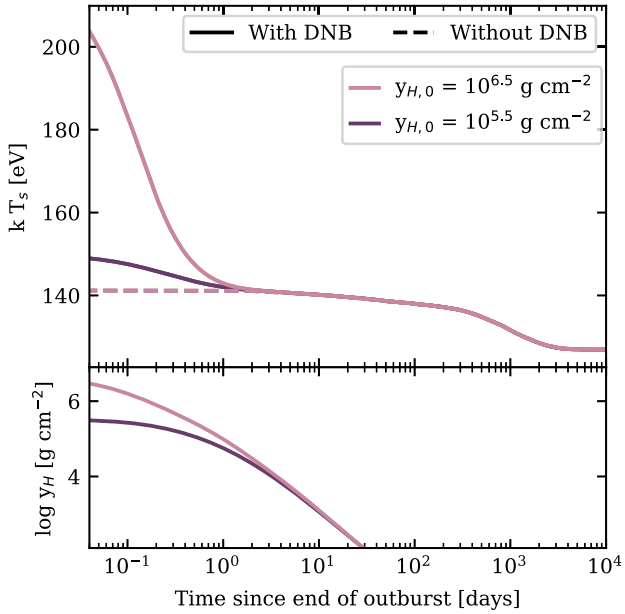


**Figure 7.** Comparison of the post-outburst surface temperature evolution with (solid) and without (dashed) additional DNB heating for different initial hydrogen columns (see line colours). The interior luminosity was calculated using an outburst duration of 10 yr and $\dot{M} = 10^{17}\,\mathrm{g\,s^{-1}} \approx 2 \times 10^{-9}\,\mathrm{M_\odot\,yr^{-1}}$.

For a given $M$ and $R$, the nuclear burning luminosity for an H–C envelope can be calculated as a function of $T_\mathrm{b}$ and $y_\mathrm{H}$ (analogue to Fig. 3). Before we can calculate the nuclear burning luminosity for a given $T_\mathrm{b}$, we convert the surface temperature, $T_\mathrm{s,old}$, to the corresponding $T_\mathrm{b}$ using the analytic envelope relations for an H–C envelope described in Section 2.1.

### 4.1 Effect on cooling curves due to heat generation

In Figs 6 and 7, we show the resulting surface temperature evolution for an accretion outburst duration of 1 and 10 yr, respectively, with constant accretion rates. As the amount of heat deposited on the star during the outburst is sensitive to the outburst duration and accretion rate, we vary either one of these parameters to obtain varying interior luminosity strengths after the outburst. We compare the surface temperature with and without DNB for two initial hydrogen columns and use the burning rate at each time step to evolve the hydrogen column size.

Figs 6 and 7 clearly show that the importance of DNB depends sensitively on the initial hydrogen column after the accretion outburst, as this sets the amount of hydrogen available for burning. For initial hydrogen columns $<3.2 \times 10^5$ g cm$^{-2}$, the change in surface temperature due to DNB is <5 per cent. For larger initial hydrogen columns ($y_\mathrm{H} \gtrsim 3.2 \times 10^6$ g cm$^{-2}$), which are typically assumed in cooling studies for a solar mixture of light elements, the initial change in surface temperature is >5–50 per cent depending on the interior luminosity strength set by the accretion history. In the following, we discuss the low and high post-outburst luminosity scenarios for the case when the cooling starts with a large initial hydrogen column ($\log y_\mathrm{H}$ [g cm$^{-2}$] = 6.5).

Fig. 6 corresponds to the scenario of a relatively short accretion period, resulting in low post-outburst cooling luminosities and surface temperatures. Despite the relatively low temperatures, $T^0_\mathrm{s,old} = 1.2 \times 10^6$ K (corresponding to $kT_\mathrm{s} = 103$ eV), when there is a substantial hydrogen column, the heating due to DNB is large and increases the initial post-outburst surface temperature by ∼19 per cent to $T^0_\mathrm{s} \sim 1.4 \times 10^6$ K (corresponding to $kT_\mathrm{s} = 120$ eV). The absolute increase in initial surface temperature is $\Delta T_\mathrm{DNB} = 2.2 \times 10^5$ K. For these temperatures, the duration of higher surface temperatures due to heat released by DNB is ∼10 d.

For longer accretion outbursts, which result in higher post-outburst luminosities (see Fig. 7), the initial increase in surface temperature due to DNB is larger (when the initial hydrogen column is large enough, $y_\mathrm{H} \gtrsim 1.2 \times 10^6$ g cm$^{-2}$). In this case, the initial surface temperature increases by 47 per cent corresponding to an absolute increase in temperature of $\Delta T_\mathrm{DNB} = 7.7 \times 10^5$ K. This means that the initial surface temperature has increased from $T^0_\mathrm{s,old} = 1.6 \times 10^6$ K (corresponding to $kT_\mathrm{s} = 141$ eV), to $T^0_\mathrm{s} \sim 2.4 \times 10^6$ K (corresponding to $kT_\mathrm{s} = 204$ eV). However, higher post-outburst luminosities lead to shorter durations (∼hours to days) when DNB contributes significantly to the total luminosity and surface temperature. The total amount of energy available from burning hydrogen is set by the initial hydrogen column, and corresponds to the integral of the elevated luminosity cooling curves, which is constant in all cases with the same initial hydrogen column. For the initial hydrogen column of $y_\mathrm{H} \sim 1.2 \times 10^6$ g cm$^{-2}$, the total amount of energy that is released from hydrogen burning is $10^{38}$ erg (i.e. ∼7 MeV nucleon$^{-1}$).

Without residual accretion or a large helium buffer that may slow down the depletion of hydrogen, the times when DNB significantly increases the observed surface temperature for an H–C envelope are ∼0.1–80 d from the end of the accretion outburst, depending on the initial hydrogen column and cooling luminosity. For larger initial cooling luminosities (and thus higher surface temperatures), the initial change in surface temperatures increases, while the relevant duration decreases, as the available hydrogen is consumed more rapidly.

### 4.2 Effect on cooling curves due to changing composition

In addition to releasing energy through nuclear reactions, DNB can alter the observed cooling after accretion outbursts by altering the light element column in the envelope over time. In Section 2.1, we show the effect on the $T_s$–$T_b$ temperature relations for varying hydrogen column sizes in H–C envelopes (see Fig. 1). The decreasing hydrogen column due to DNB will only affect the cooling curve when the hydrogen column is varied in the transition region (as shown in Fig. 2). At the relevant temperatures for NSs in quiescence (with initial post-outburst surface temperatures $T_s > 8 \times 10^5$ K), this means that the same boundary temperature (at the bottom of the envelope) corresponds to different surface temperatures when the hydrogen column varies in the range $10^4 \lesssim y_H \lesssim 10^7$ g cm$^{-2}$. When the initial hydrogen column after the accretion outburst is smaller than $y_H \sim 10^4$ g cm$^{-2}$, a further decreasing hydrogen column will not affect the cooling curve. When the initial hydrogen column is larger than $y_H \sim 10^4$ g cm$^{-2}$, the cooling curve transitions from relatively hydrogen-rich envelope temperature relations towards those for a hydrogen-poor envelope. We show this effect in Fig. 8, where we ignore the effect of heat released by DNB and only show the effect of a changing envelope composition. The dashed cooling curves in Fig. 8 correspond to fixed hydrogen columns, while the solid cooling curves correspond to the scenario where the hydrogen column decreases over time due to DNB. When DNB is taken into account, all the plotted cooling curves (irrespective of initial column density) correspond to that of a hydrogen-poor envelope after ∼50 d. Note that for larger post-outburst luminosities, it can take less time (∼1 d) to decrease the hydrogen column below $y_H \sim 10^4$ g cm$^{-2}$ (see e.g. the bottom panel in Fig. 7).

Currently, the unknown post-outburst envelope composition introduces an uncertainty in cooling models through the $T_s$–$T_b$ relations and is often left as a free fit variable. By taking into account DNB, it is possible to further constrain the post-outburst envelope composition, although the initial composition that is left after the accretion outburst is still uncertain. Regardless of the initial hydrogen column, we find that our cooling curves correspond to the hydrogen-poor limit within ∼100 d.

## 5 APPLICATION TO CRUST COOLING SOURCES

In this section, we calculate cooling curves including DNB for observed crust cooling sources in LMXBs. We select sources for which shallow heating was invoked in order to explain the observed temperatures (see Section 1). We model the sources without shallow heating to show how the quiescent heating due to DNB compares to observations. We use the method described in Section 4, but include the time variable accretion rate described in Ootes et al. (2016) to estimate the effect of DNB luminosity on cooling curves.

### 5.1 Aql X-1

The NS in the Aquila X-1 (Aql X-1) LMXB displays frequent accretion outbursts with typical durations of a few months (see e.g. Waterhouse et al. 2016). Because of its frequent outbursts, Aql X-1 is a promising source for the study of shallow heating during outbursts. Ootes et al. (2018) modelled its thermal evolution for the period between 1996 and 2015, which includes 23 accretion outbursts. They found that the observed cooling after multiple outbursts could be explained using different magnitudes and depths of the shallow heating source. New temperature data for the cooling

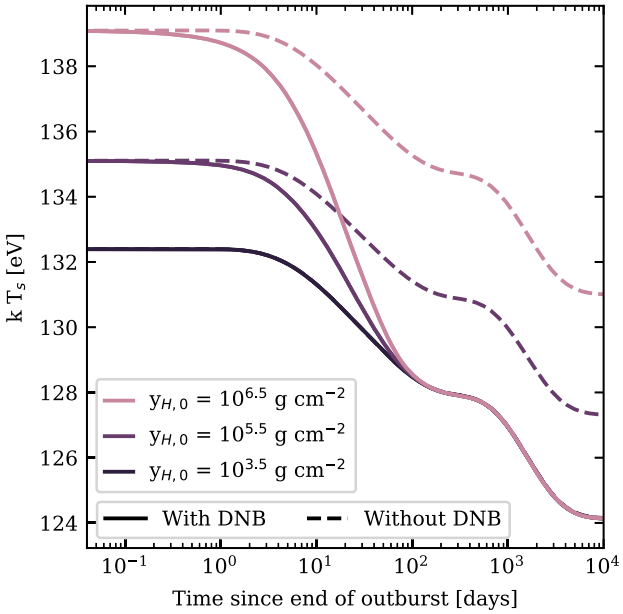


**Figure 8.** The effect of a changing hydrogen column due to DNB (while ignoring heat release, see text) on the post-outburst surface temperature evolution for different (initial) hydrogen columns (see line colours). The interior cooling was calculated using an outburst duration of 1 yr and $\dot{M} = 10^{17}$ g s$^{-1}$ $\approx 2 \times 10^{-9}$ M$_\odot$ yr$^{-1}$.

after its 2016 outburst were presented by Degenaar et al. (2019), who further investigated the shallow heating properties by comparing the cooling after its 2011, 2013, and 2016 outbursts. The three outbursts showed a striking similarity in outburst properties such as duration, peak flux, and overall shape, but were followed by cooling tracks with very distinct differences in the early time thermal evolution. Degenaar et al. (2019) found that the depth and magnitude of the shallow heating source during the 2016 outburst must have been larger than during the 2013 outburst.[1] This indicates that the shallow heating properties can be different after multiple similar outbursts in the same source. Here, we briefly explore an alternative scenario for the differences in the early time cooling curves by calculating the heating effect from DNB of accreted hydrogen.

We use NSCOOL to calculate an illustrative cooling model that loosely follows the inferred temperatures after the 2016 outburst and the late-time cooling of the 2011 and 2013 outbursts. We do not attempt to find a best-fitting model, as we only intend to investigate whether a cooling model with the same NS, accretion, and shallow heating properties could explain the observed differences at early times. We use a mass and radius of $M = 1.6$ M$_\odot$ and $R = 11$ km, which are consistent with those used in the spectral fits to obtain the temperature data (Ootes et al. 2018; Degenaar et al. 2019). As the three outbursts had similar durations and accretion rates, we use an average accretion rate of $\dot{M} = 10^{18}$ g s$^{-1}$ for an outburst duration of 2.5 months. Our model assumes a core temperature of $T_{core} = 1.1 \times 10^8$ K and includes a shallow heating source of $Q_{shallow} = 1.3$ MeV nucleon$^{-1}$ at a maximum depth of $\rho = 2.5 \times 10^{10}$ g cm$^{-3}$.

In Fig. 9, we compare the inferred temperatures after the three outbursts to the cooling track given by our model (dashed line)

[1]No strong constraints could be placed on the shallow heating properties during the 2011 outburst due to the lack of observations during the early cooling phase <80 d (Ootes et al. 2018; Degenaar et al. 2019).

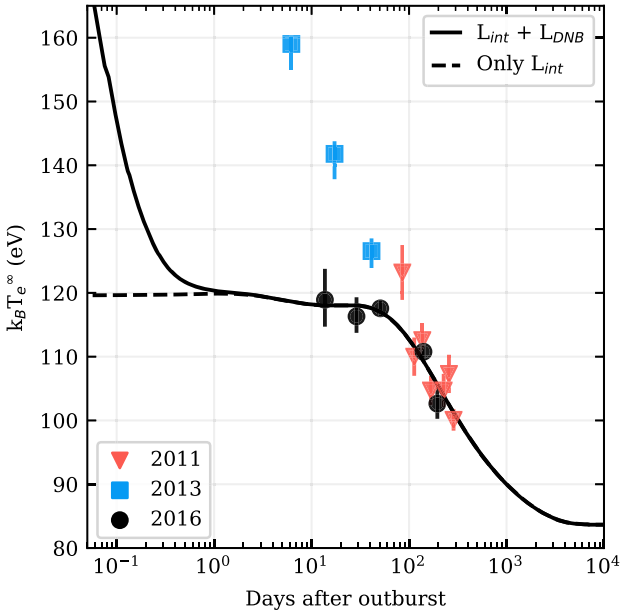


**Figure 9.** Illustrative cooling curves for the neutron star (NS) in Aql X-1 compared to the inferred temperatures after its 2011 (red triangles), 2013 (blue squares), and 2016 (black circles) outbursts. The cooling curves in this graph correspond to the same cooling model with the same NS properties. The differences between the curves are due the absence/presence of DNB. The dashed line shows a cooling model that includes a shallow heat source with $Q_{\rm shallow} = 1.3$ MeV nucleon$^{-1}$. The solid line shows the same cooling model when heating due to DNB is included. As the hydrogen column is quickly depleted at these temperatures, the DNB luminosity is only relevant <1 d.

and the track given by the same model when luminosity from DNB is added (solid line). When including the DNB luminosity, we assume an initial hydrogen column after the outburst of $y_{\rm H} = 1.2 \times 10^6$ g cm$^{-2}$. We find that, due to the high temperatures, the hydrogen column drops rapidly to $y_{\rm H} = 3.2 \times 10^4$ g cm$^{-2}$ within 1 d and no significant luminosity is produced by DNB after that time. Therefore, the cooling curves with and without a DNB luminosity are the same after 1 d and DNB of hydrogen alone does not explain the observed differences up to 80 d into the cooling. It is also unlikely that the differences in early time cooling between the outbursts can be explained with DNB and residual low-level accretion, as the accretion rates required produce a luminosity that would dominate the total observed luminosity.

Note that in all our cooling curves including DNB, we made the assumption that the generated heat immediately leaves the star at the surface and has no effect on the interior cooling. Therefore, the cooling curves are only affected during active DNB. An inwards heat flow could potentially prolong the time-scale over which DNB affects the cooling curve when accretion is not included, as the heat will reach the surface at later times. However, as the heat is produced at shallow depths, this effect is expected to be small.

### 5.2 MAXI J0556−332

The cooling after the 2012 outburst of MAXI J0556−332 is the most extreme case for which shallow heating has been invoked. The temperatures after the end of the outburst are by far the hottest ever observed. A very large amount of shallow heating, ∼15 MeV nucleon$^{-1}$, was necessary during the outburst to explain the observed cooling after the outburst was over (Homan et al. 2014; Deibel et al. 2015; Parikh et al. 2017), which is about an order of magnitude more than what was needed for other sources. Interestingly, for the cooling after two subsequent reheating outbursts in this source, much less shallow heating was needed (Parikh et al. 2017).

We discuss DNB in relation to this source, as it poses the most extreme scenario in terms of both shallow heating and large post-outburst temperatures. In fact, the source is so hot that besides proton captures on to carbon, another nuclear reaction needs to be included. At temperatures below $10^8$ K, a result of the proton capture on to C is the creation of $^{13}$N, which decays into $^{13}$C. At temperatures $T > 10^8$ K, the time in which $^{13}$N captures hydrogen is shorter than the time in which it decays, thus adding another reaction in which additional heat is released. Therefore, we also include the second step of the hot CNO cycle, such that the hydrogen capturing reactions are

$$\mathrm{H}_1^1 + \mathrm{C}_6^{12} \rightarrow \mathrm{N}_7^{13} + \gamma, \tag{4}$$

$$\mathrm{H}_1^1 + \mathrm{N}_7^{13} \rightarrow \mathrm{O}_8^{14} + \gamma, \tag{5}$$

where the second reaction deposits an additional amount of energy in the envelope (i.e. 4.63 MeV per reaction).

We find that, even with the inclusion of hydrogen captures on to nitrogen, DNB alone does not produce enough heat by far to explain the large observed temperatures observed in MAXI J0556−332. At these temperatures, the burning rate is so high that large accretion rates are required to maintain the hydrogen column at levels at which enough heat is produced. Even with the inclusion of decaying low-level accretion rates after the outburst, we find that very large initial accretion rates ($\dot{M}_{\rm init} \sim 10^{15}$ g s$^{-1}$) are required to reach the observed post-outburst temperatures. These accretion rates can be ruled out, as the corresponding accretion luminosity ($\sim 10^{35}$ erg s$^{-1}$) would be significantly larger than the observed luminosity. We also consider a possible He–C envelope, as the conditions are suitable for helium burning. However, we find that while a large helium column ($y_{\rm He} \sim 10^{12}$ g cm$^{-2}$) will increase the temperature during the full cooling time, the shift is not large enough to explain the observed temperatures. Smaller helium columns will not make a significant contribution to heat generation (see luminosity in Fig. 3).

In Fig. 10, we show the relative change in column size for varying initial light element columns. For H–C envelopes, we find that all hydrogen is rapidly depleted within ∼20 d, regardless of the initial column size after the accretion outburst. For He–C envelopes, where only helium that penetrates deep in the envelope is consumed by captures on to heavier elements, the helium column can decrease but is not completely consumed in the crust cooling time. It is interesting that observations of a hydrogen atmosphere in this source may be evidence for the presence of low-level accretion in quiescence as all initial hydrogen would be consumed within 20 d. Note that only a small accretion rate is needed to regain a hydrogen atmosphere (see Chang & Bildsten 2004; Wijngaarden et al. 2019 for a discussion on the effect of DNB on the composition of the atmosphere).

We note that other nuclear reactions may be taking place that are currently unaccounted for. Liu et al. (2017) calculate cooling curves for MAXI J0556−332 without shallow heating but including the full $\beta$-decay limited hot CNO cycle and while assuming a decaying accretion rate during quiescence. In their calculation, nuclear burning does not occur diffusively but follows a fixed burning rate for the hot CNO cycle (independent of the amount of hydrogen available and the density) in the region of the envelope where $T > 10^9$ K and changes in abundances are not taken into account. They conclude that the hot CNO cycle can significantly

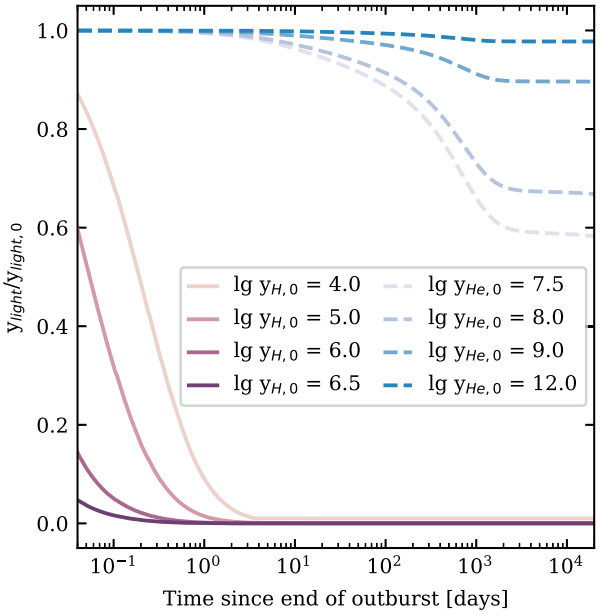


**Figure 10.** Evolution of the light element column through DNB of MAXI J0556−332 for hydrogen (in an H–C envelope) and helium (in an He–C envelope) for varying initial column sizes. All initial hydrogen is consumed in the H–C envelope, while initially large helium column sizes decrease but remain present despite the relatively large temperatures.

increase the surface temperature and find that the hot CNO cycle operates up to ∼500 d into quiescence. However, as we show here, when changes in abundance are taken into account (i.e. hydrogen depletion due to nuclear burning) the increase in luminosity due to hydrogen burning effectively shuts off much sooner (within 20 d if no further accretion takes place).

## 6 DISCUSSION

### 6.1 General effects of DNB

We study the effect of DNB on observed NS crust cooling in three ways: (i) by obtaining static temperature relations for H–C envelopes that include DNB (Section 2.1); (ii) by considering the additional heating due to DNB (Section 4.1); and (iii) by considering time variable light element columns (Section 4.2). It is typically assumed that no heat is generated in the NS envelope during quiescence, but here we find that the DNB luminosity is not always negligible. Specifically, the DNB luminosity is relevant in H–C envelopes for hydrogen columns $\gtrsim 10^5$ g cm$^{-2}$ at surface temperatures $\gtrsim$1 MK, and for He–C envelopes for helium columns $\gtrsim 10^{11}$ g cm$^{-2}$ at surface temperatures $\gtrsim$2 MK. Thus, the surface luminosity can be dominated by DNB for relevant parts of the parameter space (see Fig. 3) that can affect the interpretation of early time surface temperature observations. However, as the light element column decreases rapidly, the DNB luminosity is only relevant at times within ∼80 d after the outburst for low post-outburst temperatures and within ∼1 d for larger post-outburst temperatures (see Section 4).

We find that the conditions in quiescent NSs in LMXBs are such that active DNB can rapidly decrease the light element column size on relatively short time-scales (within ∼1–100 d). Good data sampling in the early phases (<50–100 d) are necessary to see the effects. This result can be relevant for crust cooling studies, as the $T_s$–$T_b$ relations are not fixed for one column size during the time the crust cools back to thermal equilibrium with the core. Instead, the $T_s$–$T_b$ relations change accordingly when the light element column size decreases in the transition region (see Fig. 2). This could manifest in two ways.

(i) For cooler post-outburst temperatures, the hydrogen column is consumed at a lower rate and the corresponding change in $T_s$–$T_b$ relations is potentially observable as an initial decrease in surface temperature at $\lesssim$80 d after the end of the outburst (see Fig. 8). This initial cooling is dominated by the change in composition and thus transparency of the envelope, rather than cooling of the interior.

(ii) For hotter post-outburst temperatures, the hydrogen column is consumed at a sufficiently short time-scale (within hours to a few days) such that the full observable cooling curve corresponds to a static, hydrogen-poor envelope. Limits on the envelope composition due to rapid DNB at early times can be used to constrain the static envelope composition at later times if the post-outburst accretion rate is assumed to be negligible for replenishing the light element column in the sensitivity strip.

Our main conclusion is that the current static treatment of the NS envelope during thermal evolution studies, even on the short time-scales considered in cooling studies, may not be appropriate. Processes such as DNB can significantly alter the envelope composition over time and can release additional heat, making it worthwhile to include the burning region of the envelope in future thermal evolution calculations. This would require setting the upper boundary of thermal transport equations to lower densities than $\rho_b = 10^8$ or $10^{10}$ instead of using static temperature relations to connect the temperature at those densities to the temperature at the surface (see Beznogov, Page & Ramirez-Ruiz 2020 for a more consistent treatment of the envelope applied to young NSs).

### 6.2 DNB as shallow heating mechanism?

We find that DNB can increase the initial post-outburst surface temperatures to even larger values than the observed initial temperature, without invoking an unknown shallow heat source. However, the temperature increase due to DNB drops too rapidly (<10 d) to explain the large observed surface temperatures at 50–100 d for Aql X-1. We find that without an additional shallow heating source, large accretion rates are necessary to replenish the hydrogen column that would produce an X-ray luminosity that would dominate the total luminosity. Therefore, DNB of hydrogen alone is not able to lift the need for an additional shallow heating source during the outbursts of Aql X-1. DNB in both H–C and He–C envelopes cannot replace shallow heating for MAXI J0556−332, the source with the most extreme post-outburst temperatures (see Section 5.2). The large post-outburst accretion rates needed to match these temperatures with DNB would overwhelm diffusive burning and produce accretion luminosities that are larger than the observed luminosity.

The amount of shallow heating has been found to differ between sources and even after multiple outbursts in the same source. Nuclear burning could generate different amounts of additional heating for different post-outburst envelope compositions (which depend on the accretion history). We examine whether including both DNB and shallow heating for multiple Aql X-1 outbursts (i.e. the 2011, 2013, and 2016 outbursts from Ootes et al. 2018; Degenaar et al. 2019) could lift the need for a varying amount of shallow heating between outbursts. We find that at the inferred post-outburst temperatures, the hydrogen in the envelope would be consumed

within 1 d and DNB no longer produces a significant luminosity at the time of the cooling observations. Furthermore, the required accretion rates to replenish the hydrogen column sufficiently to explain the early time cooling observations are expected to produce accretion luminosities much larger than the observed luminosity.

It would be interesting to include nuclear burning in the envelope both during the accretion outburst (non-diffusive burning) and in quiescence (diffusive burning), as potential heat flow into the NS interior is currently not accounted for and could extend the time when DNB is relevant. The work presented here involves calculating independently the evolutions of interior luminosity, DNB luminosity, and size of light element column. It would be worthwhile to perform a self-consistent calculation, which includes a cooling code outer boundary condition that can vary with the burning region. Such a study could also include a full nuclear reaction network to evolve the envelope composition beyond two-component models considered here and in previous works.

## ACKNOWLEDGEMENTS

MJPW thanks the organizers and participants of the ICONS 2019 meeting in Amsterdam for useful presentations and discussions that contributed to this paper. WCGH acknowledges support through grant ST/R00045X/1 from Science and Technology Facilities Council in the UK. We acknowledge the support of the PHAROS COST Action (CA16214). LSO and RW are supported by an NWO Top Grant, module 1, awarded to RW. DP and MB acknowledge financial support by the Mexican Consejo Nacional de Ciencia y Tecnología with a CB-2014-1 grant #240512. MB also acknowledges support from a postdoctoral fellowship from DGAPA, UNAM. This research made use of NumPy (Van Der Walt, Colbert & Varoquaux 2011), SciPy (Jones et al. 2001), and matplotlib, a PYTHON library for publication quality graphics (Hunter 2007).

## REFERENCES

Beznogov M. V., Page D., Ramirez-Ruiz E., 2020, ApJ, 888, 97
Beznogov M. V., Potekhin A. Y., Yakovlev D. G., 2016, MNRAS, 459, 1569
Brown E. F., Bildsten L., Chang P., 2002, ApJ, 574, 920
Brown E. F., Bildsten L., Rutledge R. E., 1998, ApJ, 504, L95
Brown E. F., Cumming A., 2009, ApJ, 698, 1020
Brown E. F., Cumming A., Fattoyev F. J., Horowitz C. J., Page D., Reddy S., 2018, Phys. Rev. Lett., 120, 182701
Chamel N., Haensel P., 2008, Living Rev. Relativ., 11, 10
Chang P., Bildsten L., 2003, ApJ, 585, 464
Chang P., Bildsten L., 2004, ApJ, 605, 830
Chang P., Bildsten L., Arras P., 2010, ApJ, 723, 719
Cumming A., Brown E. F., Fattoyev F. J., Horowitz C. J., Page D., Reddy S., 2017, Phys. Rev. C, 95, 025806
Degenaar N. et al., 2014, ApJ, 791, 47
Degenaar N. et al., 2019, MNRAS, 488, 4477
Deibel A., Cumming A., Brown E. F., Page D., 2015, ApJ, 809, L31
Gudmundsson E. H., Pethick C. J., Epstein R. I., 1983, ApJ, 272, 286
Haensel P., Zdunik J. L., 1990, A&A, 227, 431
Homan J., Fridriksson J. K., Wijnands R., Cackett E. M., Degenaar N., Linares M., Lin D., Remillard R. A., 2014, ApJ, 795, 131
Hunter J. D., 2007, Computing In Science & Engineering, 9, 90
Jones E. et al., 2001, Open source scientific tools for Python
Liu H., Matsuo Y., Hashimoto M.-a., Noda T., Fujimoto M. Y., 2017, J. Phys. Soc. Jpn., 86, 123901
Merritt R. L. et al., 2016, ApJ, 833, 186
Ootes L. S., Page D., Wijnands R., Degenaar N., 2016, MNRAS, 461, 4400
Ootes L. S., Wijnands R., Page D., Degenaar N., 2018, MNRAS, 477, 2900
Page D., 2016, Astrophysics Source Code Library, record ascl:1609.009
Page D., Reddy S., 2013, Phys. Rev. Lett., 111, 241102
Parikh A. S. et al., 2017, ApJ, 851, L28
Potekhin A. Y., Chabrier G., Yakovlev D. G., 1997, A&A, 323, 415
Potekhin A. Y., Pons J. A., Page D., 2015, Space Sci. Rev., 191, 239
Potekhin A. Y., Yakovlev D. G., Chabrier G., Gnedin O. Y., 2003, ApJ, 594, 404
Van Der Walt S., Colbert S. C., Varoquaux G., 2011, Computing in Science & Engineering, 13, 22
Waterhouse A. C., Degenaar N., Wijnands R., Brown E. F., Miller J. M., Altamirano D., Linares M., 2016, MNRAS, 456, 4001
Wijnands R., Degenaar N., Page D., 2017, J. Astrophys. Astron., 38, 49
Wijngaarden M. J. P., Ho W. C. G., Chang P., Heinke C. O., Page D., Beznogov M., Patnaude D. J., 2019, MNRAS, 484, 974

## APPENDIX A: ANALYTIC $T_S$–$T_B$ RELATIONS

In this section, we present accurate fits to the computed $T_s$–$T_b$–$y_H$ data that can be used in cooling simulations. All the fits are obtained for an envelope with surface gravity $g_{s,0} = 2.4271 \times 10^{14}$ cm s$^{-2}$ but can be scaled for any $g_s$ using $Y = (T_s/1\ \mathrm{MK})(g_{s,0}/g_s)^{1/4}$ (Gudmundsson et al. 1983). We use an adapted version of the analytic functions (equation A1) presented by Beznogov et al. (2016):

$$T_b(Y, y_H) = 10^7\ \mathrm{K} \left( f_4(Y) + [f_1(Y) - f_4(Y)] \times \left[ 1 + \left( \frac{y_H}{f_2(Y)} \right)^{f_3(Y)} \right]^{-0.2} \right). \quad \text{(A1)}$$

The analytic relation fitted for the H–C mixture for an envelope with a lower boundary of $\rho_b = 10^{10}$ g cm$^{-3}$ is given by equation (A1) that consists of the functions (A2). Here, the functions $f_1$–$f_4$ are identical to those for the He–C mixture in Beznogov et al. (2016). The best fit parameters are given in Table A1. We obtain a maximum relative error of 0.016. The root mean square of the relative error is 0.0037:

$$f_1(Y) = p_1 Y^{p_2 \log_{10} Y + p_3},$$
$$f_2(Y) = p_7 Y^{p_8 (\log_{10} Y)^2 + p_9},$$
$$f_3(Y) = p_{10} \sqrt{\frac{Y}{Y^2 + p_{11}^2}},$$
$$f_4(Y) = p_4 Y^{p_5 \log_{10} Y + p_6}. \quad \text{(A2)}$$

This paper has been typeset from a TEX/LATEX file prepared by the author.